Identifying forecast uncertainties for biogenic gases in the Po valley related to model configuration in EURAD-IM during PEGASOS 2012

Annika Vogel[1,2,a] and Hendrik Elbern[1,2]

[1]Institute for Energy and Climate Research - Troposphere (IEK-8), Forschungszentrum Jülich, Germany
[2]Rhenish Institute for Environmental Research at the University of Cologne, Germany
[a]now also at: Institute for Geophysics and Meteorology, University of Cologne, Germany

Correspondence: A.Vogel (av@eurad.uni-koeln.de)

Abstract. Forecasts of biogenic trace gases in the planetary boundary layer (PBL) are highly affected by simulated emission- and transport processes. The Po region during the PEGASOS campaign in summer 2012 provides challenging, yet common, conditions for simulating biogenic gases in the PBL. This study identifies and quantifies principal sources of forecasts uncertainties induced by various model configurations under these conditions. Specifically, effects of model configuration on different processes affecting atmospheric distributions of biogenic trace gas distributions are analyzed based on a priori available information. The investigation is based on the EURAD-IM chemistry transport model employing the MEGAN 2.1 biogenic emission module and RACM-MIM as gas phase chemistry mechanism. Two major sources of forecast uncertainties are identified in this study. Firstly, biogenic emissions appear to be exceptionally sensitive to land surface properties inducing total variations of local concentrations of up to one order of magnitude. Moreover, these sensitivities are found to be highly similar for different gases and almost constant during the campaign, varying only diurnally. Secondly, the model configuration also highly influences regional flow patterns with significant effects on pollutant transport and mixing. This effect was corroborated by diverging source regions of a representative airmass and thus applies also to non biogenic gases. As a result, large sensitivities to model configuration are found for surface concentrations of isoprene as well as OH, affecting reactive atmospheric chemistry. Especially in areas with small scale emission patterns, changes in the model configuration are able to induce significantly different local concentrations. The amount and complexity of sensitivities found in this study demonstrate the need to consider forecast uncertainties of chemical transport models with special focus on biogenic emissions and pollutant transport.

1 Introduction

One of the major challenges in tropospheric chemistry modeling is the skillful simulation of biogenic compounds, comprising emission, atmospheric transport, chemical reaction, and deposition. Being actively evolved in the formation of secondary organic aerosol (SOA, e.g., Geng et al., 2011; Shrivastava et al., 2017) and the photochemical production of tropospheric ozone (e.g., Geng et al., 2011; Wu et al., 2015), biogenic volatile organic compounds (BVOCs) have a significant impact on trace gas and aerosol composition. However, important BVOCs like isoprene show a large spatio-temporal variability which

hampers the investigation of regional to global effects (e.g., Mentel et al., 2013). As biogenic emissions dependent on various environmental conditions, forecasts of biogenic gases are exceptionally sensitive to the model setup like parameters and input fields.

Emili et al. (2016) claim that an investigation of major sources of forecast uncertainties is required before forecast errors can be estimated. Generally, atmospheric chemical forecasts are highly affected by a large number of model inputs and parameters, including the meteorological forcing. In this regard, Zhang et al. (2012b) state that more effort is needed on how meteorology and model setup affect chemical forecasts. Chemistry transport models (CTMs) are driven by numerical weather prediction (NWP) forecasts and thus inherit their errors. Different meteorological input from different NWP models or different setups of the NWP model are found to influence chemical forecasts significantly (e.g., Hu et al., 2010; Zhang et al., 2012a; Vogel et al., 2020). In addition, CTMs are sensitive to information on the earths surface type and vegetation distribution as well as emission maps (e.g., Ma and van Aardenne, 2004; Chen et al., 2014). The formulation of aerosol uptake and reactive chemistry may also serve as important components of the model configurations (e.g., Zhang et al., 2012c; Gama et al., 2019; Chen et al., 2019).

Concerning biogenic gases, highly complex dependencies of the emission process induce exceptionally large sensitivities to various model configurations including land use information and meteorological conditions (e.g. Wang et al., 2017; Henrot et al., 2017). These complex dependencies result in large differences in modeled biogenic emissions on a global scale. Focusing on climate related dependencies, Arneth et al. (2011) investigated global annual changes in modeled isoprene emissions due to climatology and vegetation input. Although the authors identified substantial effects of model input on globally averaged emissions, their results indicated increased sensitivity and complexity on smaller scales.

On regional and local scales, modeled trace gas distributions are increasingly influenced by boundary layer dynamics which controls advection and mixing of airmasses (e.g., Eder et al., 2006; Zhang et al., 2012b; Banks et al., 2016). An example of highly complex chemistry-turbulence interactions is found by Kaser et al. (2015) who investigated effects of local separation of isoprene and OH. The large spatio-temporal gradients of observed biogenic gases renders regional forecasts highly sensitive to both, local emission- and flow patterns. Furthermore, forecast evaluation of biogenic gases is limited by exceptionally sparse observations suitable for comparison to CTM forecasts (e.g., Arneth et al., 2008; Guenther et al., 2012). This is the more the case, as available in situ observations of biogenic VOCs are hardly representative for an area larger than a few kilometers which are numerically resolved by CTMs. Ideally, hardly available free boundary layer probing under well mixed conditions may allow for reliable model evaluation.

In summer 2012, high-resolution observations of chemical distributions in the planetary boundary layer (PBL) were performed in the Po valley during the PEGASOS campaign (*Pan-European Gas-AeroSOls-climate interaction Study*, $http://pegasos.iceht.forth.gr/$). The Po valley is known to be one of the most polluted regions in Europe (e.g., Sogacheva et al., 2007; Israelevich et al., 2012; Finardi et al., 2014; Kontkanen et al., 2016; Sandrini et al., 2016). Firstly, this region is highly populated (Finardi et al., 2014) with associated high anthropogenic emissions from traffic, industry and power plants (e.g., Kontkanen et al., 2016). Emission hotspots in urban areas like Bologna and Modena are surrounded by agricultural areas with various emission characteristics. Moreover, heterogeneous and highly patchy agricultural surface patterns are likely to remain unresolved in regional models with some kilometers grid spacing. Secondly, the topography of the Po valley impedes

mixing and exchange of polluted airmasses on a regional scale (e.g., Sogacheva et al., 2007). This is mainly due to the Alps in the north and west and the Apennine Mountains in the southwest, framing the valley at three sides. The inner Po valley is characterized by a flat topography, supporting the development of nocturnal inversion layers during cloud free nights (Li et al., 2014). Thus, the Po valley is expected to provide challenging conditions with respect to local emission patterns and regional transport processes.

In the framework of the PEGASOS Po valley campaign 2010, a number of studies focus on in situ observations of aerosol composition (e.g., Wolf et al., 2015; Sullivan et al., 2016; Kontkanen et al., 2016; Rosati et al., 2016b; Bucci et al., 2018; Karnezi et al., 2018). Some findings point towards potential difficulties in simulating low level transport and biogenic gases in this region. According to Wolf et al. (2015) and Rinaldi et al. (2015), different local transport patterns affected observed aerosol composition in this region. Rosati et al. (2016a) found different aerosol properties in distinct coexisting layers within the evolving morning boundary layer. Regarding biogenic VOCs, Kaiser et al. (2015) observed low concentrations in the Po valley during the campaign. Additionally, Karnezi et al. (2018) found that the largest variation in simulated overall SOA during the campaign was induced by biogenic SOA components. Overall a dedicated quantitative assessment study on forecast uncertainties of biogenic trace gases prior to SOA- and ozone formation is as yet missing.

In this context, airborne observations from the PEGASOS campaign allow a detailed evaluation of simulated biogenic gases. However, effects of individual model configurations on forecasts should be taken into account when evaluating the forecast model and estimating related uncertainties. The main goal of this study is to identify and quantify principal sources of forecast uncertainties by evaluating effects of different model configurations on atmospheric chemical processes. Here, the evaluation does not refer to a quantitative forecast evaluation with respect to observations. Instead we aim to analyze out the pathways of the simulated differences in order to better understand their impact. With this approach, differences in simulated concentrations can be traced back to specific model configuration options affecting different parts of the modeling system. Thus, this study provides a precursory step prior to comprehensive forecast validation by observations as well as probabilistic simulations. Focusing on biogenic gases, various kinds of sensitivities related to model input and setup are considered, including the configuration of the meteorological model. Other potential sources of uncertainties related to chemical conversions are not investigated in this study.

Section 2 gives an overview over the context of this study including the meteorological situation during the campaign and the selection of specific cases. The modeling system and important model configurations are described in Sect. 3. The evaluation of sources of forecast uncertainties in the Po valley during the PEGASOS campaign 2012 is performed in two steps. Firstly, effects of model configurations on biogenic emissions, pollutant transport and dry deposition are analyzed (Sect. 4). In the context of pollutant transport, calculating source areas of airmasses allows for a detailed analysis of modeled airmass history with respect to transport and mixing processes. Secondly, the effects of these model processes are analyzed in terms of differences in local trace gas concentrations (Sect. 5).

The results focus on a set of biogenic gases with different dependencies on the model processes to demonstrate differences and similarities between gases. Isoprene is a directly emitted biogenic VOC with comparably short atmospheric lifetime. Methanol is part of the model variable "HC3" which also includes ethanol and propane as not biogenically emitted alkanes.
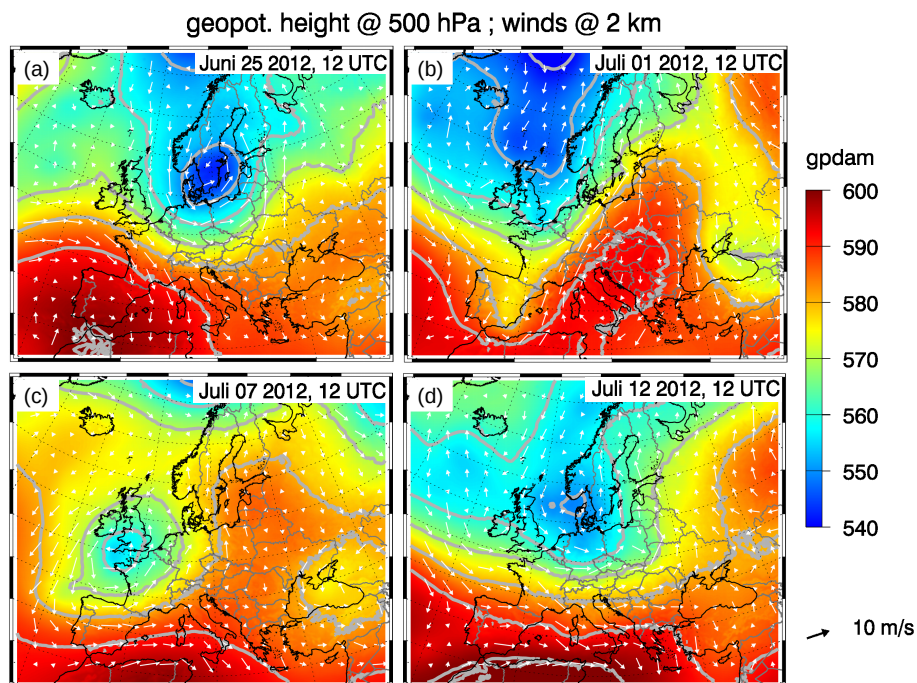
Figure 1. Geopotential height at 500 hPa (color coded+isolines) and horizontal winds at 2 km height (arrows) during the PEGASOS campaign in Po valley as simulated by WRF (initialized with IFS reanalysis, setup denoted as "reference" later on).

The model variable "aldehyde" represents a composite of oxidized BVOCs which are affected by several processes including biogenic- and anthropogenic emissions, photochemical production, atmospheric transport and dry deposition. Detailed results in Sect. 4 and Sect. 5 are given for a single case on 12 July 2012. Introducing dominant uncertainties to the model, generalized sensitivities of biogenic emissions during the campaign are presented in Sect. 6. Finally, Sect. 7 evaluates the effects of different model configurations and concludes consequences for model evaluation and uncertainty estimation.

2   Case Study Description

The PEGASOS campaign in the Po valley took place from 18 June to 13 July 2012. A Zeppelin NT (*New Technology*) served as airborne observational platform sampling the PBL during 22 flights over the Po valley. A detailed documentation of the Zeppelin's measurement configurations during the campaigns in 2012 is available from Jäger (2013). Section 2.1 gives a short overview over the synoptic scale meteorological conditions during the campaign. The averaged daily evolution of local meteorological quantities observed at San Pietro Capofiume (SPC) during the campaign is given in Kontkanen et al. (2016). Specific cases which are identified to be representative for this study are described in Sect. 2.2.

2.1 Meteorological Conditions

During June and July 2012, the synoptic situation in Europe was influenced by Rossby wave activity as shown in Fig. 1. Eastward moving troughs force several low pressure systems to move across central and northern Europe. Nevertheless, the weather in the Po valley was continuously influenced by southern high pressure systems.

At the very beginning of the campaign, a large trough over the Atlantic ocean induced south-westerly flow over Europe. The trough detached from the polar vortex and moved north-eastwards towards southern Sweden during the next days. On 25 June 2012, large pressure gradients between this low pressure system and a high pressure system over the Strait of Gibraltar forced strong north-westerly to westerly winds over central Europe (Fig. 1(a)). Under these conditions, the Alpine Mountains act as orographic barrier resulting in low wind speeds in the leeward Po valley. These calm conditions are confirmed by radio sounding in SPC from the Italian Meteorological Service (Servizio Meteorologico). During the next days, the low- and high pressure systems weakened and moved eastwards towards the Black Sea. On 01 July 2012, a trough extended from the British Islands towards Spain, causing south-westerly flow over central Europe (Fig. 1(b)). The trough was connected to several surface lows and frontal activity inducing cloudy and rainy conditions from Spain to Poland and Finland. Being separated by the Alps, the weather in northern Italy was still influenced by the weakened high pressure system in the east. Thus, clear and partly foggy conditions with calm winds and and temperatures above $20°C$ were observed in the Po valley during the morning hours on 01 July 2012.

The trough and its controlling low pressure systems propagated north-east bound during the next days. Subsequently, a cut-off low developed south of Iceland and started to separate from the polar vortex on 04 July 2012. Three days later, on 07 July 2012, the center of the cut-off low was located over the British Islands (Fig. 1(c)). Again, a cold front over Poland influenced the local weather north of the Alps but did not affect the Po region. Instead, slow varying winds from south-western to north-western directions and clear sky conditions have still been observed in the Po valley by the Italian Meteorological Service. These conditions in the Po valley persisted until the end of the campaign on 13 July 2012. During this time, the cut-off low has weakened and reconnected to the polar vortex. On 12 July 2012, a new trough was formed and moved towards the North Sea (Fig. 1(d)) along with a sequence of associated surface lows. Additionally, a large high pressure system formed over north-western Africa which directed westerly flow towards south-western Europe.

Radiosonde observations at San Pietro Capofiume (SPC) from the Italian Meteorological Service are launched at 00 UTC each day. On 12 July 2012, the sounding states calm conditions with westerly winds of about $1.5 \mathrm{~m \, s^{-1}}$ to $5 \mathrm{~m \, s^{-1}}$ in the lowest $100 \mathrm{~m}$. The temperature at 00 UTC was $21.2°C$ close to the surface with a temperature inversion reaching up to $26.8°C$ in $200 \mathrm{~m}$ height. At this time, the relative humidity reduces steadily from 69% to 42% in about $1 \mathrm{~km}$ height. These local conditions are sufficiently well simulated by the WRF forecasts for all model configurations used in this study at 00 UTC. Simulated surface near winds are between $2.5 \mathrm{~m \, s^{-1}}$ and $5.5 \mathrm{~m \, s^{-1}}$ from south-western directions, relative humidity close to the surface ranges from 50% to 69% and temperatures vary between $21.3°C$ and $24.6°C$. All simulations capture the inversion, but tend to underestimate its intensity as maximum temperatures in $200 \mathrm{~m}$ height are about $25°C$.

2.2 Selected Cases

The set of observational instruments onboard the Zeppelin was deployed following the emphasis assigned to each individual PEGASOS flight (see e.g. Jäger, 2013, for an overview). Flight patterns are either vertical profiles by helical flight patterns close to the base station at SPC or horizontal transects to different parts of the Po valley. Flight number *F049* on 12 July 2012 is an example for a helical flight pattern which was performed close to Argenta. With a radius of about 1 km, the Zeppelin spanned altitudes from 50 m up to 750 m above ground between 03:20 and 09:20 UTC. In contrast, horizontal transects were performed to the central Po valley, the Adriatic Sea as well as the Apennine Mountains. During some of the flights to the Apennine Mountains – like flight number *F039* on 01 July 2012 – the Zeppelin followed a large valley towards Monte Cimone (2165 m a.s.l.). Most of the flights took place in the early morning hours to investigate the morning development of the mixed boundary layer. Only on 07 July 2012, flight number *F045* was scheduled between 17:00 and 20:20 UTC to investigate effects of the weakening vertical mixing during the evening hours.

This study focuses on three different cases during the PEGASOS Po valley campaign: (1) early morning on 01 July 2012, (2) evening on 07 July 2012, and (3) early morning on 12 July 2012. The selection is made upon the differences in synoptic conditions, time of day and flight pattern in order to cover different principal conditions during the campaign. Thus, these cases allow for a generalized analysis of averaged sensitivities in the Po valley during the campaign. From these, special emphasis is placed on the early morning hours on 12 July 2012, which has already been selected for other studies (Li et al., 2014; Kaiser et al., 2015). It appears to be a typical case for investigating chemical components during the development of a morning mixed layer during this campaign.

3 Modeling System

The atmospheric chemical simulations are performed by the EURAD-IM modeling system, which will be introduced in Sect. 3.2. As the meteorological simulation provides an important set of model inputs, the numerical weather prediction model WRF serving as meteorological driver for EURAD-IM is shortly described in Sect. 3.1. Finally, Sect. 3.3 describes the selected model inputs and configurations which are considered during this study. For all selected cases, the simulations of WRF and EURAD-IM are initialized one day before the day of evaluation at 00 UTC, each. Thus, at least 27 hours of spin-up are performed for all meteorological and chemical fields in addition to the initialization of meteorological fields including soil moisture in WRF. Both models share the same domain and projection which is Lambert conformal with 15 km horizontal spacing (compare Fig. 1). Based on this, a 5 km and the final 1 km domain are driven by initial- and boundary conditions from their respective mother domains. The vertical layers are defined by terrain following σ coordinates with 23 levels extending up to 100 hPa for both models.

3.1 WRF numerical weather prediction

The WRF (*Weather Research and Forecasting*) model is a mesoscale numerical weather prediction model, devised by a joint coordination effort of NCAR (National Center for Atmospheric Research), NOAA (National Oceanic and Atmospheric Administration), the U.S. Air Force, the Naval Research Laboratory, the University of Oklahoma and the Federal Aviation Administration. In this study, the advanced research WRF (WRF-ARW) version 3.8.1 is used (Skamarock et al., 2008). WRF-ARW solves a fully compressible non hydrostatic formulation of the prognostic equations. Time integration is performed by 2nd or 3rd order Runge-Kutta schemes. The vertical grid is defined by terrain following hydrostatic pressure coordinates and the prognostic variables are horizontally staggered in an Arakawa-C-grid (Arakawa and Lamb, 1977) stencil. For a detailed description of WRF-ARW 3.8.1 see Skamarock et al. (2008).

Multiple schemes for various kinds of parameterizations are implemented in WRF-ARW. Available parameterizations account for subgrid scale processes related to the boundary- and surface layer, land- and urban surface, lake physics, short- and longwave radiation, cloud microphysics and cumulus parameterizations. Effects of these parameterizations on atmospheric chemical forecasts are investigated in this study. The selection of parameterization schemes is given in Sect. 3.3. A detailed description of the available parameterization schemes can be found in Skamarock et al. (2008).

3.2 EURAD-IM chemistry transport model

The atmospheric chemical data assimilation system EURAD-IM (*EURopean Air pollution Dispersion - Inverse Model*) combines a state-of-the-art chemistry transport model with spatio-temporal data assimilation and inversion methods (Elbern et al., 2007). The chemistry transport model within EURAD-IM provides forecasts of a large set of gas phase and aerosol compounds up to lower stratospheric levels (e.g., Hass et al., 1995). Considered transformation processes include dynamical transformations due to advective and diffusive processes as well as reactive chemistry with other compounds and photolysis. For this study, the RACM-MIM (*Regional Atmospheric Chemistry Mechanism,* Geiger et al., 2003) mechanism for reactive chemistry is selected which considers 221 chemical- and 23 photolysis reactions of 84 gases including condensed isoprene degradation (*Mainz Isoprene Mechanism* MIM, Pöschl et al., 2000).

Emissions from anthropogenic- and biogenic sources are treated separately, where anthropogenic emissions are provided by the TNO-MACC-II inventory (Kuenen et al., 2014). The MEGAN 2.1 (*Model for Emissions of Gases and Aerosols from Nature version 2.1*, Guenther et al., 2012) module is used for biogenic emissions from urban, natural, and agricultural sources. In total, 147 chemical compounds are considered, which are grouped into 19 classes according to their emission properties. For each of these component classes, vegetation dependent emissions are calculated from standard emissions, multiplied by the local vegetation fraction. These vegetation dependent emissions are scaled by an activity factor to account for variations in the environmental conditions. According to Guenther et al. (2012), effects of radiation, temperature, leaf age, soil moisture, and CO_2 are included in a multiplicative manner. Therefore, required input parameters include fields of plant functional types (PFT), leaf area index (LAI), solar radiation, air temperature, and soil moisture.

Table 1. Selection and description of considered model input sources. PX = Pleim-Xiu surface layer parameterization, Du = Dudhia short-wave radiation parameterization. For further information on parameterization schemes in WRF see e.g Skamarock et al. (2008). Increased roughness lengths are based on Berndt (2018).

input source	selected options		description
	reference	alternative	
global meteo	IFS	GFS	global meteorological forecasts for initial- and boundary conditions in WRF
land use	USGS	MODIS	land use information (spatial distribution of PFT, LAI) in WRF and EURAD-IM
land surface	Pleim-Xiu	RUC	land surface model in WRF
boundary layer	MYJ + Eta	ACM2 + PX	boundary layer- and surface layer parameterization schemes in WRF
microphysics	WSM6	TGS	cloud microphysics parameterization scheme in WRF
radiation	RRTMG	Du + RRTM	short- and longwave radiation parameterization schemes in WRF
roughness length	original	increased	vegetation dependent roughness length (Z0) in WRF
drought response	linear	no SMOIS	decrease of biogenic emissions for low soil moisture (SMOIS)

Dry and wet deposition is implemented in the model, where wet deposition is included in the treatment of clouds. The dry deposition velocity is modeled by a multiple path resistance scheme according to Zhang et al. (2003), where aerodynamic resistance and quasi laminar sublayer resistance are a function of friction velocity (Wesely et al., 2002). In addition, different contributions to the overall canopy resistance depend on photosynthetically active radiation, air temperature, water-vapor deficit, LAI, and friction velocity.

The EURAD-IM system includes 4 dimensional variational data assimilation (*4Dvar*) for initial state and emission rate optimization (Elbern et al., 2007). This assimilation algorithm comprises an adjoint model which integrates a signal backward in time. Being implemented into the modeling system, the adjoint model can be modified to quantify the history of selected airmasses according to Vogel et al. (2020). By switching of chemical conversions, the retroplume operator allows the identification and investigation of source regions of air parcels including the convolution and mixing of different airmasses.

3.3 Model Inputs

In the following, important model configurations and their realizations selected in this study are briefly described. As summarized in Table 1, two representative realizations – a reference and an alternative option – are selected for each model configuration. Most model configurations apply to the meteorological forecasts of WRF and transfer to the atmospheric chemical forecasts via its dependencies on meteorological conditions. Firstly, initial- and boundary conditions for WRF are provided by global meteorological analyses. Here the IFS reanalysis (Hortal, 1998) provided by ECMWF is used as reference and the operational GFS analysis from NOAA (Caplan et al., 1997) serves as an alternative option.

Secondly, reference information on land surface and vegetation types are given in the form of USGS (*U.S. Geological Survey*) land use categories. In WRF, these land use information are provided by the GLCC (*Global Land Cover Characteristics*)

database. Based on AVHRR (*Advanced Very High Resolution Radiometer*) observations between April 1992 and March 1993, the surface at each location is classified as a single USGS land use category (Loveland et al., 2000). The USGS data base includes 24 different categories including water, urban, snow and ice as well as various vegetated surface categories (Anderson et al., 1976). Although the database provides unsupervised surface classification, the occurrence of different surface types is treated by mixed categories (e.g. "Cropland/Woodland Mozaic"). Vegetation products from MODIS and Sentinel-2 satellites can give more recent information on spatial distributions and also temporal evolution of vegetation types. Currently, Sentinel-2 provides vegetation products in the highest resolution (up to 10 m horizontal resolution, e.g., Immitzer et al., 2016; Drusch et al., 2012). However, these data are not available for 2012 as the satellite was launched in 2015.

Thus, fractional vegetation data with 1 km spatial resolution based on MODIS (*MODerate-resolution Imaging Spectrora-diometer*, Friedl et al., 2002) observations are transferred to land use information for this study. Multiple studies indicate a more detailed and reliable characterization compared to AVHRR based products (e.g., Hansen et al., 2002; Smirnova et al., 2016). However, GLCC land use information provide a basically different data set which has been used in a great number of studies over the last decades until today (e.g., Krinner et al., 2005; Dee et al., 2011; Sellar et al., 2019). Thus, using GLCC data from USGS as reference option provides a solid basis for investigating changes in land use information induced by MODIS. Transferring MODIS data to land use categories requires additional information on urban areas, water, snow and ice. Assuming an appropriate representation of these basic surface types, the related information of USGS were also used in the MODIS based classification. If the MODIS categories do not sum up to 100 %, the missing fraction is defined according to the USGS land use categories, if they are non zero.

Thirdly, WRF offers various options for different kinds of parameterizations. For this study, sensitivities to the land surface model (LSM), boundary- and surface layer parameterizations and cloud microphysics parameterizations as well as short- and longwave radiation parameterizations are considered. The selection of parameterization schemes is based on the frequency of usage (according to $https: //www2.mmm.ucar.edu/wrf/users/wrf\_physics\_survey.pdf$, last access on 06.04.2020) and differences in the underlying approach. For example, the two layer Pleim-Xiu (Pleim and Xiu, 1995; Xiu and Pleim, 2001) and the multi layer RUC (*Rapid Update Cycle,* Benjamin et al., 2004) schemes serve as reference and alternative option for LSM. The MYJ (*Mellor-Yamada-Janjic,* Janjic, 1994) and ACM2 (*Asymmetric Convection Model version 2,* Pleim, 2007) boundary layer parameterizations are selected because of their 1.5^{th} order local- and 1st order non local approach, respectively. As boundary- and surface layer parameterizations are closely related, the Eta-similarity (Janjic, 1996) and Pleim-Xiu (Pleim, 2006) surface layer parameterizations are selected with respect to the boundary layer parameterizations and resulting effects are investigated together. For cloud microphysics, the WSM6 (*WRF Single-Moment 6-class,* Hong and Lim, 2006) and TGS (*Thompson Graupel Scheme,* Thompson et al., 2008) parameterizations are selected. The RRTMG (*Rapid Radiative Transfer Model for GCMs,* Iacono et al., 2008) scheme is used as reference for short- and longwave radiation while alternative options are Dudhia (Dudhia, 1989) and RRTM (*Rapid Radiative Transfer Model,* Mlawer et al., 1997), respectively. No effect of cumulus parameterization schemes is investigated here because the parameterization is switched off as the 1 km domain is assumed to resolve related processes.

Finally, one additional model configuration is considered for pollutant transport and dry deposition as well as biogenic emissions, respectively. The effect of drought response to biogenic emissions introduces an important source of uncertainty. No response to soil moisture is implemented in the MEGAN 2.1 code ($http://lar.wsu.edu/megan/docs/meganv2.10\_beta.tar.gz$, last access on 09 July 2018), but Guenther et al. (2012) propose a linear reduction of isoprene emissions below a threshold soil moisture. While a general reduction of biogenic emissions under dry conditions is indicated by multiple studies, the explicit dependency of emitted gases is still under discussion (e.g., Pegoraro et al., 2004; Lavoir et al., 2009; Wu et al., 2015). Recently, Jiang et al. (2018) formulate drought response in the subsequent version MEGAN 3 as function of photosynthesis and generalized water stress. In this study, the linear decrease of emissions proposed by Guenther et al. (2012) is implemented as reference for all biogenic gases while no dependency is assumed as alternative option ("no SMOIS"). Regarding transport, Berndt (2018) indicate that predefined values of roughness length in WRF underestimate true roughness in Europe. Thus for pollutant transport and dry deposition, effects of increased vegetation dependent roughness lengths are investigated based to the values used by Berndt (2018).

4 Effects on Model Processes

Effects of different types of model inputs and configurations are investigated for biogenic emissions (Sect. 4.1), dry deposition velocities (Sect. 4.2) and pollutant transport (Sect. 4.3). This section focuses on the results for 12 July 2012, which are discussed in more detail. All three model processes discussed here are highly dependent on meteorological fields. However, using an existing meteorological ensemble appears to be not sufficient for this application. An investigation of sensitivities from the global GFS (*Global Forecast System*) ensemble from NOAA did not induce significant differences in the simulated boundary layer in this case (not shown).

4.1 Effects on Biogenic Emissions

The effects of model configurations on biogenic emissions of different gases are given in Fig. 2 and Fig 3. As the changes induced by the different model configurations are similar for all presented biogenic gases, the following description focuses on isoprene and HC3 shown in Fig. 2. Note that biogenic HC3 emissions refer solely to methanol which is the only biogenically emitted compound in this chemical group defined in the model.

Differences between nighttime (03 UTC) and daytime (09 UTC) emissions are more significant for isoprene than for other biogenic gases. This is because isoprene is a direct product of photosynthesis which is mainly limited to daytime conditions. For the reference setup ("ref"), daytime isoprene emissions are mainly restricted to the Apennine Mountains and two areas within the the central Po valley north of Modena and Bologna. According to USGS land use, these locations are assigned to "Deciduous Broadleaf Forest" and "Crop/Woodland Mosaic", respectively. In contrast to "Dryland Cropland and Pasture" in the rest of the valley, broadleaf trees emit high levels of isoprene. Thus, even small numbers of trees result in significantly increased local isoprene emissions. Biogenic emissions of alpha-pinene, limonene and aldehyde show also increased these regions, but with decreasing characteristic. In contrast, biogenic emissions of methanol and aldehydes almost equally emitted
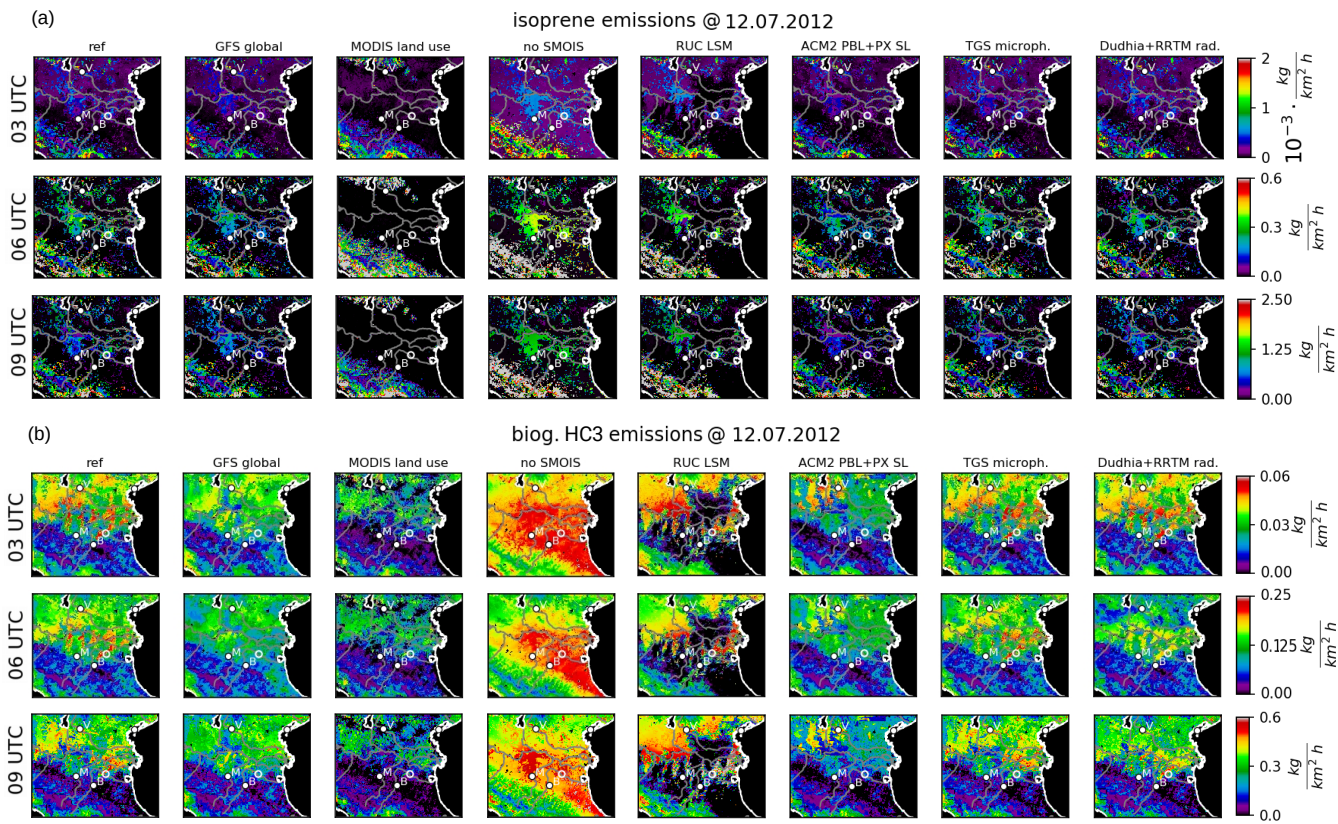
Figure 2. Isoprene (a) and biogenic HC3 (b) emissions on 12 July 2012 at 03, 06 and 09 UTC (coded by colors) for different model configurations: reference, GFS global meteorology, MODIS land use, and no response to soil dryness ("no SMOIS"), RUC LSM, ACM2 boundary layer + Pleim-Xiu surface layer schemes, TGS microphysics and Dudhia shortwave- + RRTM longwave radiation. Some important cities (Verona, Bologna, Modena) are indicated by their initial letters. The location of the Zeppelin observations on this day is given as small circle.

by all vegetation types in this regions. This results in a comparably uniform distribution over most parts of the domain with a

285   significant reduction in the Apennine mountains.

The high dependency on tree coverage is emphasized by comparing reference biogenic emissions to emissions based on MODIS land use ("land use"). In contrast to USGS, MODIS does not indicate any trees within the Po valley, which results in negligible biogenic emissions in this region. Although this effect is most prominent for isoprene, significant emission reduction is found for all considered biogenic gases. At the same time, the whole Apennine Mountains and southern foothills of the Alps

290   are assigned to high coverage of broadleaf trees resulting in high isoprene emissions. The use of GFS global meteorology does not change the general emission patterns ("global"). Caused by different initial- and boundary conditions, all biogenic emissions are slightly reduced in the whole region. The implemented response of biogenic emissions to soil dryness significantly influences biogenic emissions ("no SMOIS"). By neglecting this response, emissions are considerably larger than for the
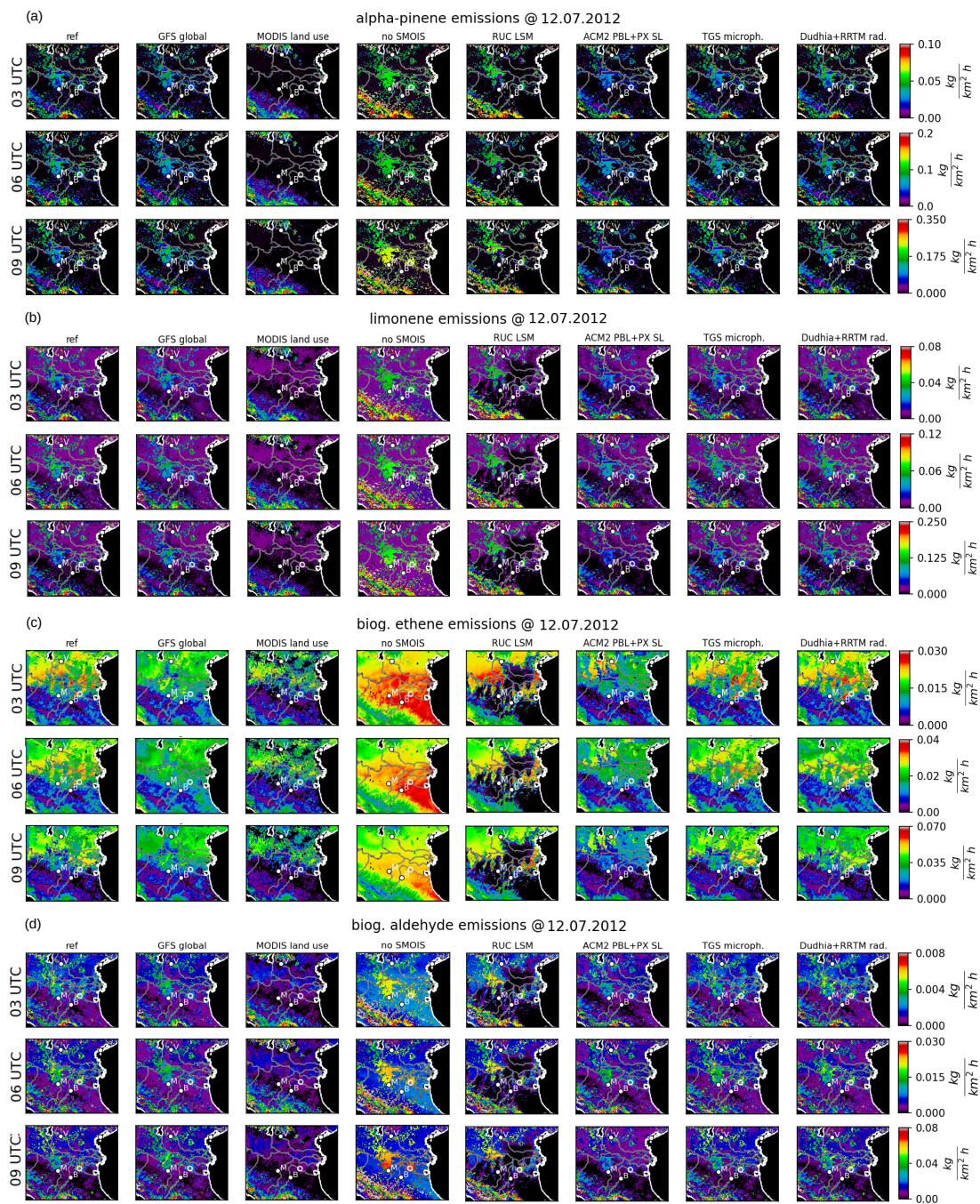
Figure 3. Alpha-pinene (a), limonene (b), biogenic ethene (c) and biogenic aldehyde (d) emissions on 12 July 2012 at 03, 06 and 09 UTC (coded by colors) for different model configurations. Plotting conventions as in Fig. 2.
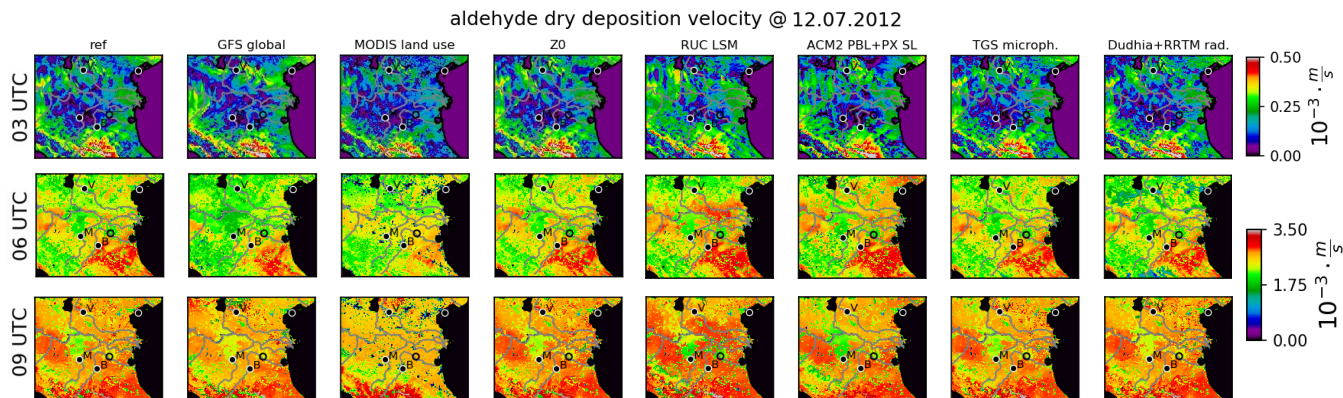
Figure 4. Dry deposition velocities of aldehyde on 12 July 2012 at 03, 06 and 09 UTC (coded by colors) for different model configurations including increased roughness length ("Z0"). Plotting conventions as in Fig. 2.

reference case, especially in the southern part of the domain. As soil moisture decreases after sunrise, the largest sensitivities
295   are found at 09 UTC for both gases.

The RUC LSM induces slightly increased biogenic emissions of all considered gases, in most areas ("LSM"). This general
increase is overlapped by a drastic reduction to almost zero emissions in the south-eastern parts of the Po valley for all gases
- most prominently visible for biogenic methanol and aldehyde emissions. This reduction is caused by low soil moisture
predicted by RUC LSM in the morning hours which results in drought induced plant stress. Using the ACM2 boundary layer-
300   (PBL) and Pleim-Xiu surface layer (SL) schemes instead of MYJ PBL + Eta SL schemes leads to a reduction of biogenic
emissions ("PBL + SL"). This effect affects the biogenic emissions of all considered gases and is largest in the eastern central
Po valley. Only minor changes in biogenic emissions due to microphysics- and radiation schemes are visible ("microph.",
"rad."). Using TGS microphysics instead of the reference WSM6 does only induce small local effects during nighttime (03
UTC). Although being small, effects of using different radiation schemes after sunrise can be attributed to different formulations
305   of shortwave radiation by the Dudhia and RRTMG schemes.

4.2   Effects on Dry Deposition Velocities

Dry deposition velocities are only investigated for aldehydes as most biogenically emitted gases are not directly dry deposited
in the model. The dry deposition velocities of aldehydes in Fig. 4 differ significantly between daytime and nighttime conditions.
While large deposition velocities are restricted to the peaks of the Apennines at 03 UTC, spatial differences reduce after sunrise.
310   In the central Po valley, aldehyde deposition velocities at 03 UTC are approximately one order of magnitude smaller compared
to 06 and 09 UTC. A small overall reduction of deposition velocities is simulated for GFS global meteorology compared to the
ECMWF reference (Fig. 4, "global"). Large differences in deposition velocities are found with respect to land use (Fig. 4, "land
use"). Most prominent is a reduction in urban areas according to USGS land use information. This is caused by an imperfect
overlap of non vegetated regions in MODIS and urban land use in USGS. In the rest of the Po valley, effects on dry deposition
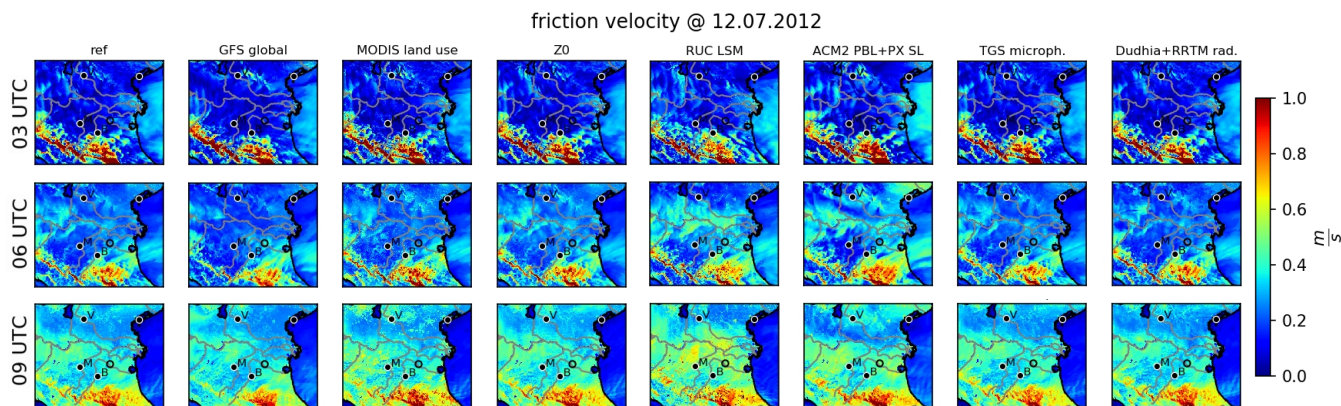
13

friction velocity @ 12.07.2012

Figure 5. Friction velocities on 12 July 2012 at 03, 06 and 09 UTC (coded by colors) for different model configurations including increased roughness length ("Z0"). Plotting conventions as in Fig. 2.

velocities point into different directions in different regions. While dry deposition is decreased in the central valley, increased values are found in the southern Apennines at 09 UTC. Increasing roughness length does slightly increase dry deposition velocities after sunrise (Fig. 4, "Z0").

Using the RUC LSM results in larger dry deposition velocities in the central Po valley at all times. Boundary layer- and surface layer schemes induces local effects with opposite signs after sunrise south of Modena and east of Verona, respectively. The selection of the microphysics schemes induces only minor local changes in this case (Fig. 4, "microph."). The largest effect of Dudhia shortwave and RRTM longwave radiation schemes appears at 06 UTC, were dry deposition velocities are decreased in the northern part of the domain (Fig. 4, "rad.").

4.3 Effects on Pollutant Transport

This section investigates effects on transport of any atmospheric pollutant. Section 4.3.1 evaluates effects on fields of friction velocity forecasted by WRF-ARW. As friction velocities only provide information on the horizontal wind speeds determining pollutant advection, source regions of airmasses indicate total effects of atmospheric dynamics. An analysis of source regions of a representative airmass is given in Sect. 4.3.2.

4.3.1 Effects on Friction Velocities

In general, friction velocities do not change substantially between night- and daytime but increase in most areas with increasing local instability. For the reference setup in Fig. 5, high values predicted at 03 UTC over the peaks of the Apennines are almost one order of magnitude higher than in the rest of the domain. After sunrise, these large differences reduce over time by increasing mean values and slightly decreasing peak values. GFS global meteorology indicates reduced friction velocities in the central Po valley especially at 06 UTC (Fig. 5, "global"). Effects of land use information appear to influence friction velocities on comparably small scales (Fig. 5, "land use"). Using MODIS instead of USGS, friction velocities are partly increased in the

14

335   north-eastern part of the domain. Friction velocities appear also to be little sensitive to increased roughness length, inducing slightly increased values after sunrise (Fig. 5, "Z0").

The selection of the LSM as well as boundary layer- and surface layer schemes induce significant effects on friction velocities (Fig. 5, "LSM" + "PBL+SL"). As early as 03 UTC, the RUC LSM triggers a region of increased values south of Lake Garda. This signal penetrates along the Po river affecting large parts of the valley from 06 to 09 UTC, resulting in almost doubled

340   friction velocities. Similar to the sensitivity to the LSM, friction velocities are partly increased in the central Po valley by the ACM2 boundary layer- and Pleim-Xiu surface layer schemes. However, this effect is less pronounced and regions of high values change with time. At the north-eastern edge north of Venice, friction velocities are increased for all times. Microphysics- and radiation parameterizations only induce minor changes in friction velocities (Fig. 5, "microph.","rad."). Slightly changed patterns due to Dudhia shortwave and RRTM longwave radiation schemes are observed in the western and eastern Po valley at

345   06 and 09 UTC, respectively.

4.3.2   Effects on Source Regions

Although differences in friction velocities do not vary substantially in this case, an investigation of the airmasses' history provides more detailed information on pollutant transport. The analysis of the meteorological conditions states the overall reproducibility of the observed local conditions by all simulations used in this study (Sect. 2.1). At the same time, the simula-

350   tions show low level variable wind directions related to the low wind speeds which might result in diverging pollutant transport. Some studies are available that investigate the history of airmasses in the Po valley by the means of long term backward trajectories (Sogacheva et al., 2007; Pernigotti et al., 2012; Sullivan et al., 2016). However, this approach does not account for local effects and related uncertainties in transport and mixing. Here, these effects are analyzed using retroplume calculations for a representative airparcel. The selected airmass is located at the position of the Zeppelin observations ($44.7°N$, $11.6°E$, "*target*

355   *location*") on 12 July 2012 at 06 UTC ("*target time*") in 100 m height above sea level. Starting at this time, the retroplume calculation provides relative contributions of source areas of this airmass backward in time. The Zeppelin observations were perfromed close to the base station of the Zeppelin at San Pietro Capofiume (SPC) in the south-eastern part of the Po valley. Being located approximately 30 km northeast of Bologna, SPC is classified as a urban background site (Kaiser et al., 2015; Rosati et al., 2016b). However, Sandrini et al. (2016) state that it might be affected by the Bologna urban area in case of

360   south-westerly winds.

Figure 6(b)+(c) show the evolution of source regions for the reference setup. The selected airmass is advected from western to north-western directions due to slow westerly winds. During the last 3 hours before the target time, the airmass converged horizontally by meredional mixing processes. Thus, contributions of this airmass converge from south-western to north-western directions at this time. 5 hours before, the major source of the airmass is found north-west of the target location. During the

365   entire time interval, the vertical extension of source areas remains below 1 km altitude (Fig. 6(c)). This is caused by low vertical mixing, which is typical for the early morning hours over flat terrain.

By applying different kinds of model configurations, resulting effects on horizontal source regions are shown in Fig. 6(a). Horizontal source areas start to diverge already during the first hours before the target time. Three hours earlier, significant
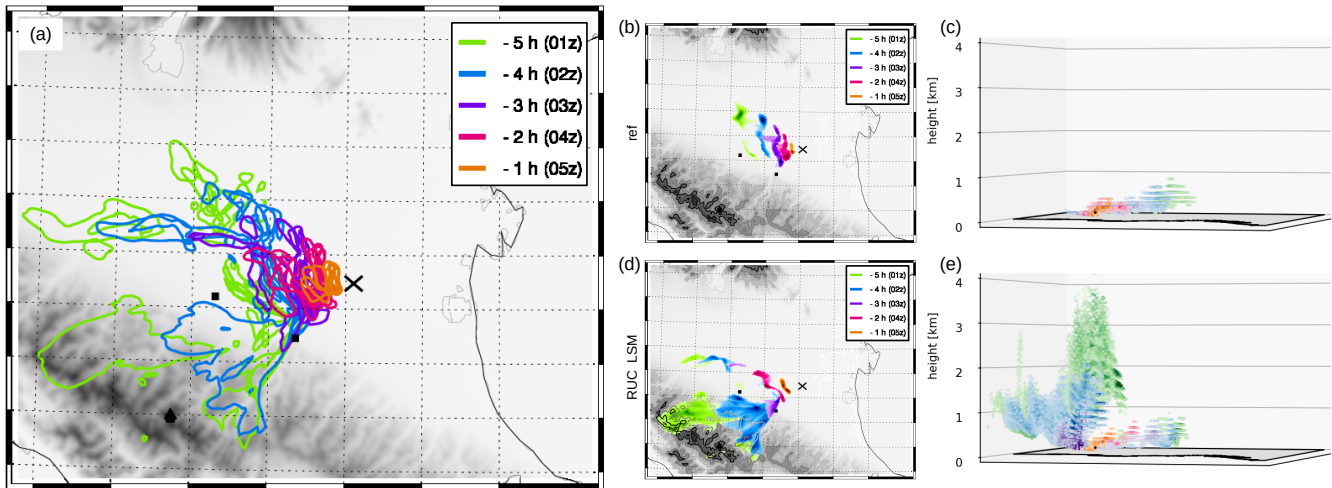
Figure 6. Horizontal ((a),(b) and (d)) and vertical ((c) and (e)) distributions of source regions for $44.7°N$, $11.6°E$ and 100 m a.s.l. (black cross, "target location") at 12 July 2012, 06 UTC. (a): Significant contributions to vertically integrated source regions for all model configurations (incl. increased roughness length) are given as isolines (colored by time according to legend). Gray colors indicate the surface topography. (b) and (c): reference configuration, (d) and (e): RUC LSM. For (b) and (d), the viewing direction is from east-northeast towards west-southwest.

contributions span from Bologna in the south-west for RUC LSM to the western central Po valley in the north-west for GFS
370　global meteorology. Five hours before, additional differences in transport distance and vertical mixing become visible. Trans-
port distances from the selected target location varies more than a factor of two at this time. For example, source regions for
the ACM2 boundary layer- and Pleim-Xiu surface layer schemes almost extend to the western boundary of the domain within
5 hours. This is caused by increased turbulent transport compared to the reference MYJ boundary layer- and Eta surface layer
schemes. In contrast, Dudhia and RRTM radiation schemes as well as MODIS land use information indicate slow horizontal
375　transport from urban areas close to Modena and Bologna. Compared to mainly agricultural source areas for the reference and
ACM2, these slight changes in local dynamics may result in significant changes in the composition of this airmass.

As shown in Fig. 6(d)+(e), the RUC LSM has the largest effect on the simulated airmass history. In the horizontal plane, a
major contribution to the airmass was transported from south-western directions crossing Bologna. Prior ti this, it descended
from the Apennine Mountains where high winds speeds advect air from comparably remote source regions. This is related to
380　increased mixing processes which result in large extended source regions 4 hours before. Between 4 and 5 hours before, the
source areas shows convergence of two distinct airmasses flowing around the highest peaks of Monte Cimone with altitudes of
more than 2000 m a.s.l. (Fig. 6(d)). The overflow above the Apennines forces the airmass to source altitudes of up to 4 km
a.s.l. 5 hours before the target time. Additionally, a small contribution of the airmass originates from a narrow valley south-west
of Bologna with lower wind speeds and source altitudes of below 1 km a.s.l. (lower left part of Fig. 6(e)).
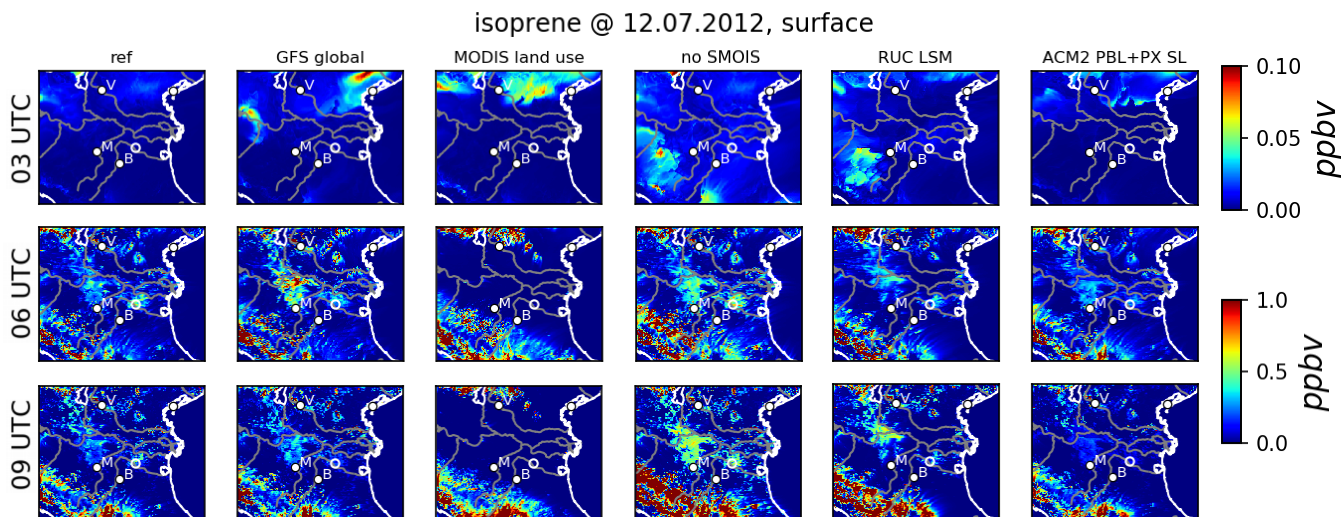
Figure 7. Isoprene surface concentrations on 12 July 2012 at 03, 06 and 09 UTC (coded by colors) for different model configurations. Plotting conventions as in Fig. 2.

5 Effects on Surface Concentrations

Simulations of surface near concentrations of trace gases are controlled by the model processes as discussed above. The evaluation of biogenic gas concentrations is restricted to isoprene because of its direct dependency on the model processes discussed above. Other biogenic gases are affected by additional processes like secondary production which hamper a detailed evaluation. Instead, resulting OH concentrations are analyzed on their impact on reactive atmospheric chemistry. As microphysics and radiation schemes appear to have only minor effects on the model processes in this case, their effects on concentrations is not further discussed.

5.1 Effects on Isoprene

Being a short lived biogenic trace gas, isoprene concentrations are mainly determined by changes in biogenic emissions as shown in Fig. 7. Consequently, effects of land use information and drought response on isoprene emissions transfer almost directly to differences in surface concentrations. Using MODIS land use produces negligible isoprene concentrations within the Po valley and increased concentrations in the mountains. An overall increase in isoprene concentrations is achieved at all times when no emission response to soil dryness is considered.

Nevertheless, effects of atmospheric transport does also influence isoprene concentrations when changing modeled global meteorology as well as LSM and boundary layer schemes. At 06 UTC, surface concentrations north of Modena are increased for GFS global meteorology although local emissions were slightly reduced (compare Sect. 4.1). This is caused by higher atmospheric stability leading to less dispersion which is indicated by reduced friction velocities (compare Sect. 4.3.1). For the RUC LSM, increased isoprene emissions are partly compensated by increased mixing in the central valley after sunrise. Thus,
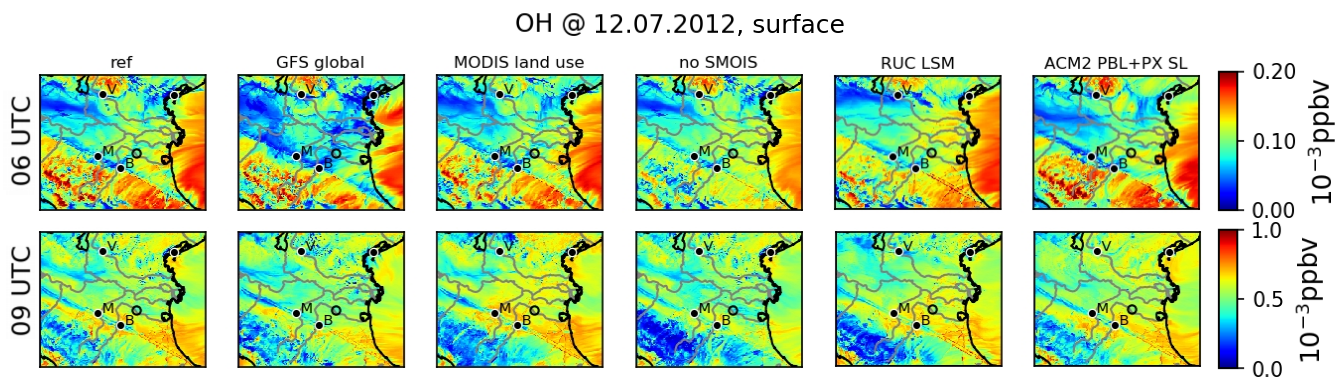
17

Figure 8. OH surface concentrations on 12 July 2012 at 06 and 09 UTC (coded by colors) for different model configurations. Plotting conventions as in Fig. 2.

the most significant increase in surface concentrations is found in the Apennine Mountains. Effects of combined boundary layer- and surface layer schemes do appear on local scales due to slightly reduced emissions and variable dynamical effects.

5.2 Effects on OH

The hydroxy radical OH is a highly reactive oxidant in the atmosphere acting as most important sink of isoprene (Kaser et al., 2015). Generally, OH may be influenced by the model configuration via reaction with biogenically emitted gases and meteorological conditions. Local meteorology mainly affects OH by changes in radiation related to humidity and clouds. In this specific case, the weather in the Po region was continuously characterized by clear and dry conditions as described in Sect. 2.1. Thus, no significant differences in humidity and cloud coverage are simulated by the model configurations (not shown). This renders the differences in OH concentrations being determined by changed biogenic VOCs.

As expected from atmospheric chemistry, daytime OH concentrations shown in Fig. 8 are reduced in regions of high BVOC concentrations like the central Po valley and the southern Apennines. In contrast, OH concentrations remain comparably high in the mountains and over the ocean were isoprene concentrations are neglectable. This direct dependence of OH to biogenic gases causes also significant differences in OH concentrations with respect to model configuration. In this case, the effects are most dominant in cases of increased isoprene concentrations with respect to the reference simulation. Significant reduction of OH is induced by excluding drought response ("no SMOIS"), RUC LSM, and less pronounced for MODIS land use in the southern Apennines. While these reductions are persistent in time, increased isoprene concentrations in the central Po valley for GFS global meteorology at 06 UTC result in temporally reduced OH concentrations in this region.

6 Generalized Effects of Biogenic Emissions

The case analysis in Sect. 4.1 indicates almost constant effects of model configurations, especially for biogenic emissions. Thus, the results can be comprised to temporally averaged sensitivities on biogenic emissions for a set of representative cases during
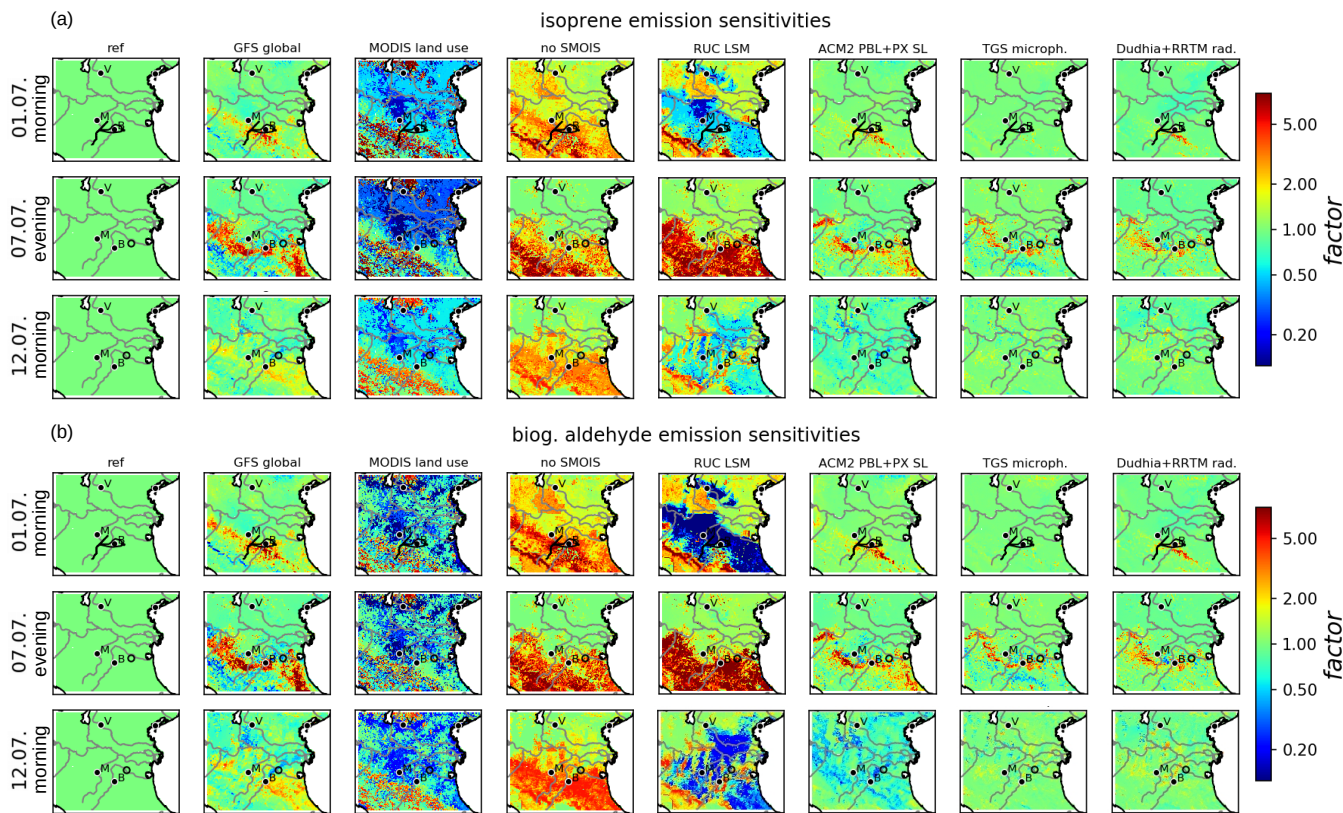
Figure 9. Averaged sensitivities on isoprene (a) and biogenic aldehyde (b) emissions on 01 July morning (00–10 UTC), 07 July evening (12–22 UTC), 12 July 2012 morning (00–10 UTC) (temporally averaged factors w.r.t. reference, coded by colors) for different model configurations. Plotting conventions as in Fig. 2.

the campaign. Sensitivity factors are calculated as temporal average of emissions at each time divided by their corresponding values from the reference configuration. While for 01 July and 12 July 2012, the analysis focuses on the morning hours between

425   00 and 10 UTC, evening conditions between 12 and 22 UTC are investigated for the 07 July 2012 case. Note that minimum emissions of $1.0 \cdot 10^{-3}$ kg km^{-2} h^{-1} are defined in order to avoid unrealistic large factors induced by low values.

As shown in Fig. 9, sensitivities of both biogenic gases during the campaign are most significant for land use, drought response and the LSM. As expected, the large averaged sensitivities to land use information are highly similar for all cases and both gases. Somehow lower averaged sensitivities on isoprene on 01 July and 12 July are induced by emissions below the

430   minimum value in the early morning. A strong increase of emissions due to neglected drought response is found for all cases, which most significant effects in the southern part of the domain.

For the two morning cases (01 July, 12 July) RUC LSM results in reduced emissions in most parts of the Po valley and increased values south of Verona and in the south-west. In contrast, highly increased biogenic emissions are produced in the entire southern half of the domain during the evening case (07 July). These diurnal differences are caused by general different

19

temporal evolutions of soil moisture, which limit biogenic emissions. While soil moisture from Pleim-Xiu LSM drops during daytime and recovers fastly during nighttime, RUC predicts a continuous decrease during these days. Thus, lower soil moisture for RUC induces lower emissions in the morning, and vise versa in the evening. Despite this general diurnal differences, sensitivities to the LSM appear to be mostly constant during the campaign.

The use of GFS global meteorology induces small, yet similar effects for all cases. While emissions are increased in the northern Apennines, emissions tend to be slightly lower elsewhere. Effects of boundary layer- and surface layer schemes remain small and differ between the cases. While for 12 July the ACM2 boundary layer- and Pleim-Xiu surface layer schemes induce decreased biogenic emissions, they produce increased emissions north of the Apennines in the other cases. Microphysics and radiation schemes induce only significant effects in the evening case (07 July) with slightly increase emissions north of the Apennines.

7   Conclusions

Forecasts of biogenic trace gases in the PBL are well known to be subject to large uncertainties. The PEGASOS campaign in the Po valley 2012 provides a challenging, yet common, environment for investigating model uncertainties with focus on biogenic gases in the PBL. As a precursory step to probabilistic model evaluation with PEGASOS observations, this study identifies and quantifies principal sources of forecasts uncertainties induced by model configurations via different model processes. Two major pathways of model uncertainties with respect to model parameters and -inputs are identified in this study:

Firstly, exceptionally large differences in simulated biogenic emissions are found in the Po valley during the campaign. Dominating impacts of land use information, the land surface model and emission response to drought state a high sensitivity of biogenic emissions to various land surface conditions. Although biogenic emissions are known to be affected by environmental conditions, these three effects induce unexpectedly high variations of up to an order of magnitude in the studied case. Due to the common approach used for modeling biogenic emissions, the results appear to be highly correlated for different biogenic gases. Moreover, these effects are found to be almost constant during the campaign, varying only with the diurnal cycle. Despite invariant vegetation distributions, this persistence is forced by steady meteorological conditions during the campaign.

Secondly, the model configuration also highly influences regional flow patterns with effects on pollutant transport and mixing. Especially the selection of land surface model and boundary layer schemes induce significant differences in local pollutant transport. Although effects on friction velocities remain small, diverging source regions prove high sensitivities of pollutant transport to the selected model configurations which applies also to non biogenic gases. Most prominent changes in horizontal advection and vertical mixing patterns induced by the land surface model can be attributed to differences in surface heat exchange. In this study, the selection of cloud microphysics and radiation schemes does only induce minor uncertainties during this study. This is due to the calm and sunny conditions in the Po valley and may be more significant for other meteorological conditions.

As a result, surface concentrations of isoprene show large sensitivities to model configuration. These sensitivities are mainly induced by changes in land use information, the land surface model and drought response via their impact on emissions. More-

20

over, changes in surface concentrations of biogenic trace gases induce significant differences in OH concentrations affecting reactive atmospheric chemistry. Excluding the emission response to drought stress reduces local OH concentrations by up to a factor of three in this study. Despite these dominant effects of biogenic emissions, highly variable transport patterns with respect to the land surface model and boundary layer schemes are likely to affect local composition significantly. Thus, especially in such areas with small scale emission patterns, the selection of the model configuration may result in highly variable local concentrations.

Although the presented results are specific for the conditions in Po valley, it can be claimed that forecasts of biogenic gases would generally benefit substantially from improved representation of the land surface. While improved land use information could be retrieved from more recent satellite products like Sentinel-2, considerably different effects of land surface models for both, biogenic emissions and pollutant transport underline the significance of soil moisture estimates for air quality modeling. Furthermore, the large amount and complexity of sensitivities found in this study demonstrate the need to account for forecast uncertainties with special focus on biogenic emissions and pollutant transport. This is especially important for model evaluation with observations as well as chemical data assimilation in the PBL. A follow up study will evaluate probabilistic model forecasts of biogenic gases using airborne PEGASOS observations of biogenic gases. In this context, the sensitivities derived in this study provide a basis for estimating forecast uncertainties with respect to different model processes.

References

Anderson, R., Hardy, E. E., Roach, J. T., and Witmer, R. E.: A land use and land cover classification system for use with remote sensor data, USGS Prof. Pap, p. 964, 1976.

Arakawa, A. and Lamb, V.: Computational design of the basic dynamical processes of the UCLA general circulation model, Methods in Computational Physics, 17, 173–265, http://www-pcmdi.llnl.gov/projects/modeldoc/amip/33ucla_fn.html, 1977.

Arneth, A., Monson, R., Schurgers, G., Niinemets, Ü., and Palmer, P.: Why are estimates of global terrestrial isoprene emissions so similar (and why is this not so for monoterpenes)?, Atmospheric Chemistry and Physics, 8, 4605–4620, 2008.

Arneth, A., Schurgers, G., Lathiere, J., Duhl, T., Beerling, D. J., Hewitt, C. N., Martin, M., and Guenther, A.: Global terrestrial isoprene emission models: sensitivity to variability in climate and vegetation, Atmospheric Chemistry and Physics, 11, 8037–8052, https://doi.org/10.5194/acp-11-8037-2011, https://www.atmos-chem-phys.net/11/8037/2011/, 2011.

Banks, R. F., Tiana-Alsina, J., Baldasano, J. M., Rocadenbosch, F., Papayannis, A., Solomos, S., and Tzanis, C. G.: Sensitivity of boundary-layer variables to PBL schemes in the WRF model based on surface meteorological observations, lidar, and radiosondes during the HygrA-CD campaign, Atmospheric Research, 176, 185–201, https://doi.org/10.1016/j.atmosres.2016.02.024, 2016.

Benjamin, S. G., Grell, G. A., Brown, J. M., Smirnova, T. G., and Bleck, R.: Mesoscale Weather Prediction with the RUC Hybrid Isentropic–Terrain-Following Coordinate Model, Monthly Weather Review, 132, 473–494, https://doi.org/10.1175/1520-0493(2004)132<0473:MWPWTR>2.0.CO;2, https://doi.org/10.1175/1520-0493(2004)132<0473:MWPWTR>2.0.CO;2, 2004.

Berndt, J.: On the predictability of exceptional error events in wind power forecasting - an ultra large ensemble approach, Ph.D. thesis, University of Cologne (Germany), 2018.

Bucci, S., Cristofanelli, P., Decesari, S., Marinoni, A., Sandrini, S., Größ, J., Wiedensohler, A., Di Marco, C. F., Nemitz, E., Cairo, F., Di Liberto, L., and Fierli, F.: Vertical distribution of aerosol optical properties in the Po Valley during the 2012 summer campaigns, Atmospheric Chemistry and Physics, 18, 5371–5389, https://doi.org/10.5194/acp-18-5371-2018, https://www.atmos-chem-phys.net/18/5371/2018/, 2018.

Caplan, P., Derber, J., Gemmill, W., Hong, S.-Y., Pan, H.-L., and Parrish, D.: Changes to the 1995 NCEP Operational Medium-Range Forecast Model Analysis Forecast System, Weather and Forecasting - WEATHER FORECAST, 12, 581–594, https://doi.org/10.1175/1520-0434(1997)012<0581:CTTNOM>2.0.CO;2, 1997.

Chen, B., Yang, S., Xu, X.-D., and Zhang, W.: The impacts of urbanization on air quality over the Pearl River Delta in winter: roles of urban land use and emission distribution, THEORETICAL AND APPLIED CLIMATOLOGY, 117, 29–39, https://doi.org/10.1007/s00704-013-0982-1, 2014.

Chen, T., Chu, B., Ge, Y., Zhang, S., Ma, Q., He, H., and Li, S.-M.: Enhancement of aqueous sulfate formation by the coexistence of NO2/NH3 under high ionic strengths in aerosol water, ENVIRONMENTAL POLLUTION, 252, 236–244, https://doi.org/10.1016/j.envpol.2019.05.119, 2019.

Dee, D. P., Uppala, S. M., Simmons, A. J., Berrisford, P., Poli, P., Kobayashi, S., Andrae, U., Balmaseda, M. A., Balsamo, G., Bauer, P., Bechtold, P., Beljaars, A. C. M., van de Berg, L., Bidlot, J., Bormann, N., Delsol, C., Dragani, R., Fuentes, M., Geer, A. J., Haimberger, L., Healy, S. B., Hersbach, H., Hólm, E. V., Isaksen, L., Kållberg, P., Köhler, M., Matricardi, M., McNally, A. P., Monge-Sanz, B. M., Morcrette, J.-J., Park, B.-K., Peubey, C., de Rosnay, P., Tavolato, C., Thépaut, J.-N., and Vitart, F.: The ERA-Interim reanalysis: configuration and performance of the data assimilation system, Quarterly Journal of the Royal Meteorological Society, 137, 553–597, https://doi.org/https://doi.org/10.1002/qj.828, https://rmets.onlinelibrary.wiley.com/doi/abs/10.1002/qj.828, 2011.

Drusch, M., Bello, U. D., Carlier, S., Colin, O., Fernandez, V., Gascon, F., Hoersch, B., Isola, C., Laberinti, P., Martimort, P., Meygret, A., Spoto, F., Sy, O., Marchese, F., and Bargellini, P.: Sentinel-2: ESA's Optical High-Resolution Mission for GMES Operational Services, Remote Sensing of Environment, 120, 25 – 36, https://doi.org/https://doi.org/10.1016/j.rse.2011.11.026, http://www.sciencedirect.com/science/article/pii/S0034425712000636, the Sentinel Missions - New Opportunities for Science, 2012.

Dudhia, J.: Numerical Study of Convection Observed during the Winter Monsoon Experiment Using a Mesoscale Two-Dimensional Model, Journal of the Atmospheric Sciences, 46, 3077–3107, https://doi.org/10.1175/1520-0469(1989)046<3077:NSOCOD>2.0.CO;2, https://doi.org/10.1175/1520-0469(1989)046<3077:NSOCOD>2.0.CO;2, 1989.

Eder, B., Kang, D., Mathur, R., Yu, S., and Schere, K.: An operational evaluation of the Eta–CMAQ air quality forecast model, Atmospheric Environment, 40, 4894–4905, https://doi.org/10.1016/j.atmosenv.2005.12.062, 2006.

Elbern, H., Strunk, A., Schmidt, H., and Talagrand, O.: Emission rate and chemical state estimation by 4-dimensional variational inversion, Atmospheric Chemistry and Physics, 7, 3749–3769, https://doi.org/10.5194/acp-7-3749-2007, http://www.atmos-chem-phys.net/7/3749/2007/, 2007.

Emili, E., Gürol, S., and Cariolle, D.: Accounting for model error in air quality forecasts: an application of 4DEnVar to the assimilation of atmospheric composition using QG-Chem 1.0, Geoscientific Model Development, 9, 3933–3959, https://doi.org/10.5194/gmd-9-3933-2016, 2016.

Finardi, S., Silibello, C., D'Allura, A., and Radice, P.: Analysis of pollutants exchange between the Po Valley and the surrounding European region, Urban Climate, 10, 682 – 702, https://doi.org/https://doi.org/10.1016/j.uclim.2014.02.002, http://www.sciencedirect.com/science/article/pii/S2212095514000121, source apportionment and modelling of urban air pollution, 2014.

Friedl, M., McIver, D., Hodges, J., Zhang, X., Muchoney, D., Strahler, A., Woodcock, C., Gopal, S., Schneider, A., Cooper, A., Baccini, A., Gao, F., and Schaaf, C.: Global land cover mapping from MODIS: algorithms and early results, Remote Sensing of Environment, 83, 287 – 302, https://doi.org/https://doi.org/10.1016/S0034-4257(02)00078-0, http://www.sciencedirect.com/science/article/pii/S0034425702000780, the Moderate Resolution Imaging Spectroradiometer (MODIS): a new generation of Land Surface Monitoring, 2002.

Gama, C., Ribeiro, I., Lange, A., Vogel, A., Ascenso, A., Seixas, V., Elbern, H., Borrego, C., Friese, E., and Monteiro, A.: Performance assessment of CHIMERE and EURAD-IM' dust modules, Atmospheric Pollution Research, 10, 1336 – 1346, https://doi.org/https://doi.org/10.1016/j.apr.2019.03.005, http://www.sciencedirect.com/science/article/pii/S1309104218306020, 2019.

Geiger, H., Barnes, I., Bejan, I., Benter, T., and Spittler, M.: The tropospheric degradation of isoprene: An updated module for the regional atmospheric chemistry mechanism, Atmospheric Environment, 37, 1503–1519, https://doi.org/10.1016/S1352-2310(02)01047-6, 2003.

Geng, F., Tie, X., Guenther, A., Li, G., Cao, J., and Harley, P.: Effect of isoprene emissions from major forests on ozone formation in the city of Shanghai, China, Atmospheric Chemistry and Physics, 11, 10 449–10 459, https://doi.org/10.5194/acp-11-10449-2011, https://www.atmos-chem-phys.net/11/10449/2011/, 2011.

Guenther, A. B., Jiang, X., Heald, C. L., Sakulyanontvittaya, T., Duhl, T., Emmons, L. K., and Wang, X.: The Model of Emissions of Gases and Aerosols from Nature version 2.1 (MEGAN2.1): an extended and updated framework for modeling biogenic emissions, Geoscientific Model Development, 5, 1471–1492, https://doi.org/10.5194/gmd-5-1471-2012, https://www.geosci-model-dev.net/5/1471/2012/, 2012.

Hansen, M. C., DeFries, R. S., Townshend, J. R. G., Sohlberg, R., Dimiceli, C., and Carroll, M.: Towards an operational MODIS continuous field of percent tree cover algorithm: examples using AVHRR and MODIS data, Remote Sensing of Environment, 83, 303–319, https://doi.org/10.1016/S0034-4257(02)00079-2, 2002.

Hass, H., Jakobs, H. J., and Memmesheimer, M.: Analysis of a regional model (EURAD) near surface gas concentration predictions using observations from networks, Meteorology and Atmospheric Physics, 57, 173–200, https://doi.org/10.1007/BF01044160, https://doi.org/10.1007/BF01044160, 1995.

570 Henrot, A.-J., Stanelle, T., Schroeder, S., Siegenthaler, C., Taraborrelli, D., and Schultz, M. G.: Implementation of the MEGAN (v2.1) biogenic emission model in the ECHAM6-HAMMOZ chemistry climate model, Geoscientific Model Development, 10, 903–926, https://doi.org/10.5194/gmd-10-903-2017, 2017.

Hong, S. and Lim, J. J.: The WRF Single-Moment 6-Class Microphysics Scheme (WSM6), J. Korean Meteor. Soc., 42, 129–151, 2006.

Hortal, M.: Formulation of the ECMWF Forecast Model, pp. 237–251, Springer Netherlands, Dordrecht, https://doi.org/10.1007/978-94-015-9137-9_10, https://doi.org/10.1007/978-94-015-9137-9_10, 1998.

575

Hu, X., Nielsen-Gammon, J., and Zhang, F.: Evaluation of three planetary boundary layer schemes in the WRF model, Journal of Applied Meteorology and Climatology, 49, 1831–1844, https://doi.org/10.1175/2010JAMC2432.1, 2010.

Iacono, M. J., Delamere, J. S., Mlawer, E. J., Shephard, M. W., Clough, S. A., and Collins, W. D.: Radiative forcing by long-lived greenhouse gases: Calculations with the AER radiative transfer models, Journal of Geophysical Research: Atmospheres, 113,
580 https://doi.org/10.1029/2008JD009944, https://agupubs.onlinelibrary.wiley.com/doi/abs/10.1029/2008JD009944, 2008.

Immitzer, M., Vuolo, F., and Atzberger, C.: First Experience with Sentinel-2 Data for Crop and Tree Species Classifications in Central Europe, Remote Sensing, 8, https://doi.org/10.3390/rs8030166, 2016.

Israelevich, P., Ganor, E., Alpert, P., Kishcha, P., and Stupp, A.: Predominant transport paths of Saharan dust over the Mediterranean Sea to Europe, Journal of Geophysical Research: Atmospheres, 117, https://doi.org/10.1029/2011JD016482, https://agupubs.onlinelibrary.wiley.
585 com/doi/abs/10.1029/2011JD016482, 2012.

Jäger, J.: Airborne VOC Measurements on board the Zeppelin NT during the PEGASOS campaigns in 2012 deploying the improved Fast-GC-MSD System, Ph.D. thesis, University of Cologne (Germany), 2013.

Janjic, Z. I.: The Step-Mountain Eta Coordinate Model: Further Developments of the Convection, Viscous Sublayer, and Turbulence Closure Schemes, Monthly Weather Review, 122, 927–945, https://doi.org/10.1175/1520-0493(1994)122<0927:TSMECM>2.0.CO;2, https://doi.
590 org/10.1175/1520-0493(1994)122<0927:TSMECM>2.0.CO;2, 1994.

Janjic, Z. I.: The Mellor-Yamada level 2.5 scheme in the NCEP Eta Model, 11th Conference on Numerical Weather Prediction, American Meteorological Society, p. 333.334, 1996.

Jiang, X., Guenther, A., Potosnak, M., Geron, C., Seco, R., Karl, T., Kim, S., Gu, L., and Pallardy, S.: Isoprene emission response to drought and the impact on global atmospheric chemistry, Atmospheric Environment, 183, 69 – 83,
595 https://doi.org/https://doi.org/10.1016/j.atmosenv.2018.01.026, http://www.sciencedirect.com/science/article/pii/S1352231018300402, 2018.

Jülich Supercomputing Centre: JURECA: Modular supercomputer at Jülich Supercomputing Centre, Journal of large-scale research facilities, 4, https://doi.org/10.17815/jlsrf-4-121-1, http://dx.doi.org/10.17815/jlsrf-4-121-1, 2018.

Kaiser, J., Wolfe, G. M., Bohn, B., Broch, S., Fuchs, H., Ganzeveld, L. N., Gomm, S., Haeseler, R., Hofzumahaus, A., Holland, F., Jaeger, J.,
600 Li, X., Lohse, I., Lu, K., Prevot, A. S. H., Rohrer, F., Wegener, R., Wolf, R., Mentel, T. F., Kiendler-Scharr, A., Wahner, A., and Keutsch, F. N.: Evidence for an unidentified non-photochemical ground-level source of formaldehyde in the Po Valley with potential implications for ozone production, Atmospheric Chemistry and Physics, 15, 1289–1298, https://doi.org/10.5194/acp-15-1289-2015, 2015.

Karnezi, E., Murphy, B. N., Poulain, L., Herrmann, H., Wiedensohler, A., Rubach, F., Kiendler-Scharr, A., Mentel, T. F., and Pandis, S. N.: Simulation of atmospheric organic aerosol using its volatility–oxygen-content distribution during the

605 PEGASOS 2012 campaign, Atmospheric Chemistry and Physics, 18, 10 759–10 772, https://doi.org/10.5194/acp-18-10759-2018, https://www.atmos-chem-phys.net/18/10759/2018/, 2018.

Kaser, L., Karl, T., Yuan, B., Mauldin III, R. L., Cantrell, C. A., Guenther, A. B., Patton, E. G., Weinheimer, A. J., Knote, C., Orlando, J., Emmons, L., Apel, E., Hornbrook, R., Shertz, S., Ullmann, K., Hall, S., Graus, M., de Gouw, J., Zhou, X., and Ye, C.: Chemistry-turbulence interactions and mesoscale variability influence the cleansing efficiency of the atmosphere, Geophysical Research Letters, 42, 10,894–
610 10,903, https://doi.org/https://doi.org/10.1002/2015GL066641, https://agupubs.onlinelibrary.wiley.com/doi/abs/10.1002/2015GL066641, 2015.

Kontkanen, J., Järvinen, E., Manninen, H. E., Lehtipalo, K., Kangasluoma, J., Decesari, S., Gobbi, G. P., Laaksonen, A., Petäjä, T., and Kulmala, M.: High concentrations of sub-3nm clusters and frequent new particle formation observed in the Po Valley, Italy, during the PEGASOS 2012 campaign, Atmospheric Chemistry & Physics, 16, 1919–1935, https://doi.org/10.5194/acp-16-1919-2016, 2016.

615 Krinner, G., Viovy, N., de Noblet-Ducoudre, N., Ogee, J., Polcher, J., Friedlingstein, P., Ciais, P., Sitch, S., and Prentice, I.: A dynamic global vegetation model for studies of the coupled atmosphere-biosphere system, GLOBAL BIOGEOCHEMICAL CYCLES, 19, https://doi.org/10.1029/2003GB002199, 2005.

Kuenen, J. J. P., Visschedijk, A. J. H., Jozwicka, M., and Denier van der Gon, H. A. C.: TNO-MACC_II emission inventory; a multi-year (2003-2009) consistent high-resolution European emission inventory for air quality modelling, Atmospheric Chemistry and Physics, 14,
620 10 963–10 976, https://doi.org/10.5194/acp-14-10963-2014, https://www.atmos-chem-phys.net/14/10963/2014/, 2014.

Lavoir, A.-V., Staudt, M., Schnitzler, J. P., Landais, D., Massol, F., Rocheteau, A., Rodriguez, R., Zimmer, I., and Rambal, S.: Drought reduced monoterpene emissions from the evergreen Mediterranean oak Quercus ilex: results from a throughfall displacement experiment, Biogeosciences, 6, 1167–1180, https://doi.org/10.5194/bg-6-1167-2009, https://www.biogeosciences.net/6/1167/2009/, 2009.

Li, X., Rohrer, F., Hofzumahaus, A., Brauers, T., Häseler, R., Bohn, B., Broch, S., Fuchs, H., Gomm, S., Holland, F., Jäger, J.,
625 Kaiser, J., Keutsch, F. N., Lohse, I., Lu, K., Tillmann, R., Wegener, R., Wolfe, G. M., Mentel, T. F., Kiendler-Scharr, A., and Wahner, A.: Missing Gas-Phase Source of HONO Inferred from Zeppelin Measurements in the Troposphere, Science, 344, 292–296, https://doi.org/10.1126/science.1248999, https://science.sciencemag.org/content/344/6181/292, 2014.

Loveland, T. R., Reed, B. C., Brown, J. F., Ohlen, D. O., Zhu, Z., Yang, L., and Merchant, J. W.: Development of a global land cover characteristics database and IGBP DISCover from 1 km AVHRR data, International Journal of Remote Sensing, 21, 1303–1330,
630 https://doi.org/10.1080/014311600210191, https://doi.org/10.1080/014311600210191, 2000.

Ma, J. and van Aardenne, J.: Impact of different emission inventories on simulated tropospheric ozone over China: a regional chemical transport model evaluation, Atmospheric Chemistry and Physics, 4, 877–887, https://doi.org/10.5194/acp-4-877-2004, 2004.

Mentel, T. F., Kleist, E., Andres, S., Dal Maso, M., Hohaus, T., Kiendler-Scharr, A., Rudich, Y., Springer, M., Tillmann, R., Uerlings, R., Wahner, A., and Wildt, J.: Secondary aerosol formation from stress-induced biogenic emissions and possible climate feedbacks,
635 Atmospheric Chemistry and Physics, 13, 8755–8770, https://doi.org/10.5194/acp-13-8755-2013, https://www.atmos-chem-phys.net/13/8755/2013/, 2013.

Mlawer, E. J., Taubman, S. J., Brown, P. D., Iacono, M. J., and Clough, S. A.: Radiative transfer for inhomogeneous atmospheres: RRTM, a validated correlated-k model for the longwave, Journal of Geophysical Research: Atmospheres, 102, 16 663–16 682, https://doi.org/10.1029/97JD00237, https://agupubs.onlinelibrary.wiley.com/doi/abs/10.1029/97JD00237, 1997.

640 Pegoraro, E., Rey, A., Greenberg, J., Harley, P., Grace, J., Malhi, Y., and Guenther, A.: Effect of drought on isoprene emission rates from leaves of Quercus virginiana Mill., Atmospheric Environment, 38, 6149 – 6156,

https://doi.org/https://doi.org/10.1016/j.atmosenv.2004.07.028, http://www.sciencedirect.com/science/article/pii/S1352231004007198, 2004.

Pernigotti, D., Georgieva, E., Thunis, P., and Bessagnet, B.: Impact of meteorology on air quality modeling over the Po valley in northern Italy, Atmospheric Environment, 51, 303 – 310, https://doi.org/https://doi.org/10.1016/j.atmosenv.2011.12.059, http://www.sciencedirect.com/science/article/pii/S1352231011013495, 2012.

Pleim, J. E.: A Simple, Efficient Solution of Flux–Profile Relationships in the Atmospheric Surface Layer, Journal of Applied Meteorology and Climatology, 45, 341–347, https://doi.org/10.1175/JAM2339.1, https://doi.org/10.1175/JAM2339.1, 2006.

Pleim, J. E.: A Combined Local and Nonlocal Closure Model for the Atmospheric Boundary Layer. Part II: Application and Evaluation in a Mesoscale Meteorological Model, Journal of Applied Meteorology and Climatology, 46, 1396–1409, https://doi.org/10.1175/JAM2534.1, https://doi.org/10.1175/JAM2534.1, 2007.

Pleim, J. E. and Xiu, A.: Development and Testing of a Surface Flux and Planetary Boundary Layer Model for Application in Mesoscale Models, Journal of Applied Meteorology, 34, 16–32, https://doi.org/10.1175/1520-0450-34.1.16, https://doi.org/10.1175/1520-0450-34.1.16, 1995.

Pöschl, U., Kuhlmann, R., Poisson, N., and Crutzen, P.: Development and Intercomparison of Condensed Isoprene Oxidation Mechanisms for Global Atmospheric Modeling, Journal of Atmospheric Chemistry, 37, 29–52, https://doi.org/10.1023/A:1006391009798, 2000.

Rinaldi, M., Gilardoni, S., Paglione, M., Sandrini, S., Fuzzi, S., Massoli, P., Bonasoni, P., Cristofanelli, P., Marinoni, A., Poluzzi, V., and Decesari, S.: Organic aerosol evolution and transport observed at Mt. Cimone (2165 m a.s.l.), Italy, during the PEGASOS campaign, Atmospheric Chemistry and Physics, 15, 11 327–11 340, https://doi.org/10.5194/acp-15-11327-2015, https://www.atmos-chem-phys.net/15/11327/2015/, 2015.

Rosati, B., Gysel, M., Rubach, F., Mentel, T. F., Goger, B., Poulain, L., Schlag, P., Miettinen, P., Pajunoja, A., Virtanen, A., Baltink, H. K., Henzing, J. S. B., Gross, J., Gobbi, G. P., Wiedensohler, A., Kiendler-Scharr, A., Decesari, S., Facchini, M. C., Weingartner, E., and Baltensperger, U.: Vertical profiling of aerosol hygroscopic properties in the planetary boundary layer during the PEGASOS campaigns, Atmospheric Chemistry and Physics, 16, 7295–7315, https://doi.org/10.5194/acp-16-7295-2016, 2016a.

Rosati, B., Herrmann, E., Bucci, S., Fierli, F., Cairo, F., Gysel, M., Tillmann, R., Groess, J., Gobbi, G. P., Di Liberto, L., Di Donfrancesco, G., Wiedensohler, A., Weingartner, E., Virtanen, A., Mentel, T. F., and Baltensperger, U.: Studying the vertical aerosol extinction coefficient by comparing in situ airborne data and elastic backscatter lidar, Atmospheric Chemistry and Physics, 16, 4539–4554, https://doi.org/10.5194/acp-16-4539-2016, 2016b.

Sandrini, S., van Pinxteren, D., Giulianelli, L., Herrmann, H., Poulain, L., Facchini, M. C., Gilardoni, S., Rinaldi, M., Paglione, M., Turpin, B. J., Pollini, F., Bucci, S., Zanca, N., and Decesari, S.: Size-resolved aerosol composition at an urban and a rural site in the Po Valley in summertime: implications for secondary aerosol formation, Atmospheric Chemistry and Physics, 16, 10 879–10 897, https://doi.org/10.5194/acp-16-10879-2016, https://www.atmos-chem-phys.net/16/10879/2016/, 2016.

Sellar, A. A., Jones, C. G., Mulcahy, J. P., Tang, Y., Yool, A., Wiltshire, A., O'Connor, F. M., Stringer, M., Hill, R., Palmieri, J., Woodward, S., de Mora, L., Kuhlbrodt, T., Rumbold, S. T., Kelley, I, D., Ellis, R., Johnson, C. E., Walton, J., Abraham, N. L., Andrews, M. B., Andrews, T., Archibald, A. T., Berthou, S., Burke, E., Blockley, E., Carslaw, K., Dalvi, M., Edwards, J., Folberth, G. A., Gedney, N., Griffiths, P. T., Harper, A. B., Hendry, M. A., Hewitt, A. J., Johnson, B., Jones, A., Jones, C. D., Keeble, J., Liddicoat, S., Morgenstern, O., Parker, R. J., Predoi, V., Robertson, E., Siahaan, A., Smith, R. S., Swaminathan, R., Woodhouse, M. T., Zeng, G., and Zerroukat, M.: UKESM1: Description and Evaluation of the UK Earth System Model, JOURNAL OF ADVANCES IN MODELING EARTH SYSTEMS, 11, 4513–4558, https://doi.org/10.1029/2019MS001739, 2019.

680 Shrivastava, M., Cappa, C. D., Fan, J., Goldstein, A. H., Guenther, A. B., Jimenez, J. L., Kuang, C., Laskin, A., Martin, S. T., Ng, N. L., Petaja, T., Pierce, J. R., Rasch, P. J., Roldin, P., Seinfeld, J. H., Shilling, J., Smith, J. N., Thornton, J. A., Volkamer, R., Wang, J., Worsnop, D. R., Zaveri, R. A., Zelenyuk, A., and Zhang, Q.: Recent advances in understanding secondary organic aerosol: Implications for global climate forcing, Reviews of Geophysics, 55, 509–559, https://doi.org/10.1002/2016RG000540, https://agupubs.onlinelibrary.wiley.com/doi/abs/10.1002/2016RG000540, 2017.

685 Skamarock, W. C., Klemp, J. B., Dudhia, J., Gill, D. O., Barker, D. M., Duda, M. G., Huang, X.-Y., Wang, W., and Powers, J. G.: A Description of the Advanced Research WRF Version 3, NCAR technical note, 2008.

Smirnova, T. G., Brown, J. M., Benjamin, S. G., and Kenyon, J. S.: Modifications to the Rapid Update Cycle Land Surface Model (RUC LSM) Available in the Weather Research and Forecasting (WRF) Model, Monthly Weather Review, 144, 1851–1865, https://doi.org/10.1175/MWR-D-15-0198.1, 2016.

690 Sogacheva, L., Hamed, A., Facchini, M. C., Kulmala, M., and Laaksonen, A.: Relation of air mass history to nucleation events in Po Valley, Italy, using back trajectories analysis, Atmospheric Chemistry and Physics, 7, 839–853, https://doi.org/10.5194/acp-7-839-2007, 2007.

Sullivan, A., Hodas, N., Turpin, B., Skog, K., Keutsch, F., Gilardoni, S., Paglione, M., Rinaldi, M., Decesari, S., Facchini, M., Poulain, L., Herrmann, H., Wiedensohler, A., Nemitz, E., Twigg, M., and Jr, J.: Evidence for ambient dark aqueous SOA formation in the Po Valley, Italy, Atmospheric Chemistry and Physics, 16, 8095–8108, https://doi.org/10.5194/acp-16-8095-2016, 2016.

695 Thompson, G., Field, P. R., Rasmussen, R. M., and Hall, W. D.: Explicit Forecasts of Winter Precipitation Using an Improved Bulk Microphysics Scheme. Part II: Implementation of a New Snow Parameterization, Monthly Weather Review, 136, 5095–5115, https://doi.org/10.1175/2008MWR2387.1, https://doi.org/10.1175/2008MWR2387.1, 2008.

Vogel, A., Ungermann, J., and Elbern, H.: Analyzing highly uncertain source regions in the Ex-UTLS and their effects on small-scale atmospheric composition using probabilistic retroplume calculations, Atmospheric Environment, 220, 117 063,
700 https://doi.org/https://doi.org/10.1016/j.atmosenv.2019.117063, http://www.sciencedirect.com/science/article/pii/S1352231019307022, 2020.

Wang, P., Schade, G., Estes, M., and Ying, Q.: Improved MEGAN predictions of biogenic isoprene in the contiguous United States, Atmospheric Environment, 148, 337 – 351, https://doi.org/https://doi.org/10.1016/j.atmosenv.2016.11.006, http://www.sciencedirect.com/science/article/pii/S1352231016308809, 2017.

705 Wesely, M. L., Doskey, P. V., and Shannon, J. D.: Deposition parameterizations for the Industrial Source Complex (ISC3) model, https://doi.org/10.2172/1260839, 2002.

Wolf, R., Haddad, I. E., Crippa, M., Decesari, S., Slowik, J., Poulain, L., Gilardoni, S., Rinaldi, M., Carbone, S., Canonaco, F., Huang, R.-J., Baltensperger, U., and Prévôt, A.: Marine and urban influences on summertime PM2.5 aerosol in the Po basin using mobile measurements, Atmospheric Environment, 120, 447 – 454, https://doi.org/https://doi.org/10.1016/j.atmosenv.2015.09.007, http://www.sciencedirect.com/science/article/pii/S1352231015303514, 2015.

710 Wu, C., Pullinen, I., Andres, S., Carriero, G., Fares, S., Goldbach, H., Hacker, L., Kasal, T., Kiendler-Scharr, A., Kleist, E., Paoletti, E., Wahner, A., Wildt, J., and Mentel, T. F.: Impacts of soil moisture on de novo monoterpene emissions from European beech, Holm oak, Scots pine, and Norway spruce, Biogeosciences, 12, 177–191, https://doi.org/10.5194/bg-12-177-2015, https://www.biogeosciences.net/12/177/2015/, 2015.

715 Xiu, A. and Pleim, J. E.: Development of a Land Surface Model. Part I: Application in a Mesoscale Meteorological Model, Journal of Applied Meteorology, 40, 192–209, https://doi.org/10.1175/1520-0450(2001)040<0192:DOALSM>2.0.CO;2, https://doi.org/10.1175/1520-0450(2001)040<0192:DOALSM>2.0.CO;2, 2001.

27

Zhang, L., Brook, J. R., and Vet, R.: A revised parameterization for gaseous dry deposition in air-quality models, Atmospheric Chemistry and Physics, 3, 2067–2082, https://doi.org/10.5194/acp-3-2067-2003, https://www.atmos-chem-phys.net/3/2067/2003/, 2003.

720 Zhang, Y., Bocquet, M., Mallet, V., Seigneur, C., and Baklanov, A.: Real-time air quality forecasting, part I: History, techniques, and current status, Atmospheric Environment, 60, 632 – 655, https://doi.org/https://doi.org/10.1016/j.atmosenv.2012.06.031, http://www.sciencedirect.com/science/article/pii/S1352231012005900, 2012a.

Zhang, Y., Bocquet, M., Mallet, V., Seigneur, C., and Baklanov, A.: Real-time air quality forecasting, part II: State of the science, current research needs, and future prospects, Atmospheric Environment, 60, 656 – 676,

725 https://doi.org/https://doi.org/10.1016/j.atmosenv.2012.02.041, http://www.sciencedirect.com/science/article/pii/S1352231012001562, 2012b.

Zhang, Y., Chen, Y., Sarwar, G., and Schere, K.: Impact of gas-phase mechanisms on Weather Research Forecasting Model with Chemistry (WRF/Chem) predictions: Mechanism implementation and comparative evaluation, Journal of Geophysical Research: Atmospheres, 117, https://doi.org/10.1029/2011JD015775, https://agupubs.onlinelibrary.wiley.com/doi/abs/10.1029/2011JD015775, 2012c.